Eur. Phys. J. D (2012) 66: 204
DOI: 10.1140/epjd/e2012-30200-8

THE EUROPEAN PHYSICAL JOURNAL D

Regular Article

R-matrix calculations of differential and integral cross sections for low-energy electron collisions with ethanol

M.M. Fujimoto[a], W.J. Brigg, and J. Tennyson[b]

Department of Physics and Astronomy, University College London, Gower St., WC1E 6BT London, UK

Received 26 March 2012 / Received in final form 29 April 2012
Published online 16 August 2012 –

Abstract. Electron collisions with C_2H_5OH are studied up to impact energies of 10 eV using several theoretical models. Calculated differential cross sections suggest that the extrapolation to low angles used to extend experimental data and hence give integral cross sections significantly underestimates the large, dipole-driven forward scattering cross section. An improved set of values for the rotationally-unresolved elastic cross section is proposed; the corresponding rotationally resolved cross sections are also presented. Static exchange plus polarisation calculations find a very broad shape resonance in each of the $^2A'$ and $^2A''$ symmetries in the 7 eV collision region however no resonance at lower energies, in qualitative agreement with the interpretation of some but not all dissociative electron attachment measurements.

1 Introduction

Ethanol or ethyl alcohol (C_2H_5OH) is a commonly occurring and a fundamental organic molecule. It has found many uses in the environmental, industrial and commercial sectors. Particular focus has been placed on the use of ethanol as a biofuel because it can be produced from sugar cane and other crops, and because it burns well without additives with a consequent drop in environmental pollution [1,2]. Use of ethanol in internal combustion engines has brought focus onto how it behaves with electron collisions.

A variety of experimental studies on electron collisions with ethanol are available [3–10] with some corresponding theoretical work [9,11]. Of particular interest here is the joint experimental and theoretical study of Khakoo et al. [9] who present results for elastic differential cross sections at a wide range of energies from which they deduced values for the integral elastic cross section.

Ethanol is a strongly polar molecule which means that, particularly at low electron collision energies, its differential cross section is very heavily forward peaked. This makes the direct measurement of integral cross sections very challenging because of the difficulties associated with making measurements at low angles. A series of studies on electron collisions with water have shown that the best method for obtaining reliable results is to use theory to compensate for experimental issues at low collision angles [12–15]. This issue is our primary concern in the present paper. Subsequent to the completion of this work Lee et al. [16] published a joint theoretical-experimental study of elastic cross sections for methanol and ethanol. This work is largely concerned with high energies.

Besides elastic cross sections, the dominant low-energy processes in electron molecule collisions are rotational excitation, which is rarely resolved experimentally and usually considered as part of the elastic cross section, vibrational excitation (VE) and dissociative electron attachment (DEA). Ibănescu et al. [7] considered both DEA and VE in low-energy electron ethanol collisions as part of their comprehensive study on electron-induced chemistry of alcohols. Their study suggested that ethanol should display a variety of electron collision resonances. In particular their DEA spectrum showed a very weak peak at 2.88 eV, which they assigned to a very short-lived σ^* OH shape resonance. Their VE spectrum for excitation of the C–H stretch consisted of a very broad band peaking around 7.5 eV which they assigned to a short-lived σ^* CH resonance. They observed DEA bands at 6.0, 7.7 and 8.8 eV which, according to their analysis, do not have any obvious analogy in VE. They took this as providing a evidence that these bands are due to core excited Feshbach resonances. There appears to be no corresponding theoretical studies on resonances in low-energy collisions with ethanol, although we note that Ibănescu et al. supported their resonance assignments with the results of quantum chemical studies, a procedure which must be regarded as somewhat dangerous [17]. Ibănescu et al.'s results are only in partial agreement with the analysis of Orzol et al. [8] who attributed their DEA measurements to the presence of two broad resonances at about 5.5 eV and 8 eV. Identifying possible electron collision resonances is the second aim of this work.

In this paper we report R-matrix calculations of elastic and rotationally inelastic collisions with ethanol. We present both differential and integral cross sections at

[a] *Permanent address*: Universidade Federal do Paraná, Departamento de Física, 81531-990, Curitiba, Paraná, Brazil.
[b] e-mail: j.tennyson@ucl.ac.uk

energies below ethanol's ionisation threshold. Our results suggest that the published integral cross section for ethanol is too low, especially at low energies, and we propose an improved value for this cross section.

2 Calculations

2.1 The R-matrix method

The UK molecular R-matrix method we use in this work has been described carefully elsewhere [18]; thus here we just present some relevant details of the calculations. Our approach uses a single nuclear geometry but considers rotational motions of the molecule within the adiabatic nuclear rotation (ANR) approximation which should be valid for system such as ethanol with three heavy atoms at the energies considered here, 1 eV and above.

Within the R-matrix method, configuration space is divided in an inner and an outer region. The inner region is defined inside a sphere of radius a which completely contains the N-electron wave function of the target. This region is where the complicated physics occurs because at short-range all $N+1$ electrons interact strongly so that exchange and correlation effects are important. In the outer region, a one-particle wave function representing the continuum electron which moves in a local potential due to long-range interactions, such as polarisation or dipole interaction for neutral targets. In this region, no exchange or correlation effects are considered between the continuum electron and N electrons of the target.

In the Inner region, the R-matrix method represents the $N+1$ electrons wave function using a close-coupling approximation which can be written as follows [18]:

$$\Psi_k^{N+1}(x_1 \dots x_{N+1}) = \mathcal{A} \sum_{ij} a_{ijk} \phi_i^N(x_1 \dots x_N) u_{ij}(x_{N+1}) + \sum_i b_{ik} \chi_i^{N+1}(x_1 \dots x_{N+1}) \quad (1)$$

where ϕ_i^N is the target wave functions of the ith state and u_{ij} is an orbital used to represent the jth continuum electron with a partial wave expansion up to some maximum value of ℓ, $\ell_{\max}$; the subscript k denotes the kth inner region wave function; $\mathcal{A}$ is an antisymmetrisation operator introduced so that the indistinguishable inner-region electrons satisfy the Pauli principle; a_{ijk} and b_{ik} are the coefficients of expansions. The second summation in equation (1) contains functions χ_i^{N+1} which describe all $N+1$ electrons but vanish at $r = a$; thus these are described as L^2 configurations. They are included to relax the constraint of orthogonalization between scattering and target orbitals of the same symmetry.

Polarisation effect can be included in a number of ways. The simplest is via single excited L^2 configurations of the Hartree-Fock (HF) ground state wave function. In practice this involves promoting one target electron into a virtual (unoccupied target) orbital and simultaneously also placing the scattering electron into a virtual orbital generating a two-particle one-hole ($2p$, $1h$) configuration. According to the Brillouin's Theorem, these configurations do not improve the description of a HF target, but these one-electron target excitations improve the description of polarisation interactions with the continuum electron. This model is usually denoted static exchange plus polarisation (SEP). Alternative polarisation can be included via the close-coupling expansion of the first term of equation (1). In practice close-coupling calculations introduce polarisation via both terms.

In the outer region, one solves the one-particle coupled second-order differential equation for the continuum electron. The R-matrix is used to match these solutions to the inner region ones on the boundary giving the K-matrix which is used to compute other scattering observables. An important feature of ethanol is its permanent dipole moment. A Born closure procedure is used to compute the effect of the long-range interaction neglected when only partial waves from 0 to $\ell_{\max}$ are considered. In this procedure our low-ℓ T-matrices are added to analytic dipole Born T-matrices, using the ANR approximation to take account of rotational motion, and then corrected by subtracting the partial wave dipole Born contribution [19–21]. The rotationally-unresolved elastic differential cross sections are calculated using the code POLYDCS [22] which computes rotationally-resolved elastic and inelastic cross section which are then summed until convergence is achieved.

In this work, initial calculations were performed using version 4.1 of the Quantemol-N expert system [23] with more detailed studies being performed directly with the UKRMol codes [24]. As shown below, most of our calculations were performed at the SEP level, although close-coupling models were also explored.

2.2 Application to ethanol

Ethanol is a closed shell molecule with C_s symmetry in its equilibrium geometry; its ground state electronic state is $^1A'$. All calculations employed the experimentally determined trans geometry [25]; for POLYDCS rotational constants evaluated at this geometry, $A = 0.1459845$ meV, $B = 0.0390733$ meV and $C = 0.033968$ meV, were used. Target wave functions were calculated in Hartree-Fock Level, mainly using cc-pVTZ Gaussian type orbital (GTO) basis set. This gives a ground state energy of $-154.139985E_h$ and a permanent dipole moment of 1.77 D. The experimental dipole of trans ethanol is 1.44 D [26]; in practice however the energy separation between trans and gauche rotational isomers is only about 40 cm^{-1} the observed, average dipole moment of 1.69 D [27] is often used. Here we employ the trans value of 1.44 D for the long-range potential; use of the larger, average value will only serve to further increase our calculated low-angle and integral cross sections. Test calculations were also performed using cc-pVDZ and 6-311G basis sets with results essentially the same as those found below.

Coupled states calculations also used Hartree-Fock molecular orbitals but with a complete active space configuration interaction (CAS-CI) representation of the

target [28]. In this representation, 12 core electrons were kept frozen and the remaining 14 electrons were free to move in an orbital space augmented by the lowest two virtual orbitals. Given the rather limited CAS space it was decided to allow for the inclusion of extra polarisation effects by retaining extra virtual orbitals in the calculation which could be used to generate $(2p,1h)$ L^2 configurations in a fashion similar to the SEP calculations. This model introduces electronically excited states into the calculation and, in principle, allows the study of electron impact electronic excitation, although this was not pursued here.

The continuum was also represented using an expansion in GTOs. As discussed below, both standard, $\ell_{\max} = 4$, [29], and extended $\ell_{\max} = 5$ [30,31] partial wave expansions were tested. Test calculations were performed with R-matrix values $a = 10, 11, 12, 13$ and 15 a_0. Except for some lack of completeness issues with the basis sets for the larger a values, the results are not sensitive to this choice and the ones reported here all used $a = 11$ a_0.

2.3 Test studies

Having demonstrated stability with respect to changes in target basis set and R-matrix radius, the next consideration was the number of the unoccupied target orbitals (virtual orbitals) retained in the calculation. The cc-pVTZ GTO basis gives 98a′ and 63a″ virtual orbitals. Calculations at the static exchange (SE) level, not shown, found that retaining 22a′ and 13a″ orbitals was sufficient to obtain converged results. Here only one-electron excited L^2 configurations were included in the second sum of equation (1) and it produced well-converged eigenphase sums. In SE model was observed resonance in A″ symmetry near 9.6 eV.

These tests were repeated at the SEP level, see Figure 1. For an SEP calculation, virtual orbitals of both symmetries are important and these orbitals were selected in energy order. Excitations to both singlet and triplet excited states of the target were considered. At this level the eigenphase sums show considerable sensitivity to the number of virtual orbitals included. Particularly notable is the appearance of a broad resonance-like feature in the eigenphases of both symmetries as the number of these orbitals included is increased. With 35 virtual orbitals, automated Breit-Wigner fits [32] to the eigenphases gave resonance positions (widths) 8.65 (5.14) eV and 8.07 (5.75) eV for ^{2}A′ and ^{2}A″ symmetries respectively; with 55 virtual orbitals the resonances are lowered and narrowed to 8.03 (4.82) and 7.52 (5.28) eV respectively. The parameters of these exceptionally broad resonances are clearly rather sensitive to polarisation effects. Analysis of the eigenvector of the time-delay matrix [33] suggests that both of these resonances are predominantly f-wave in character. Their broadness means that they produce only very weak maxima in the elastic cross sections, even when the ^{2}A′ and ^{2}A″ symmetry contributions are inspected separately. These maxima are no longer visible once a Born correction, which significantly increases the low energy cross section, is included.

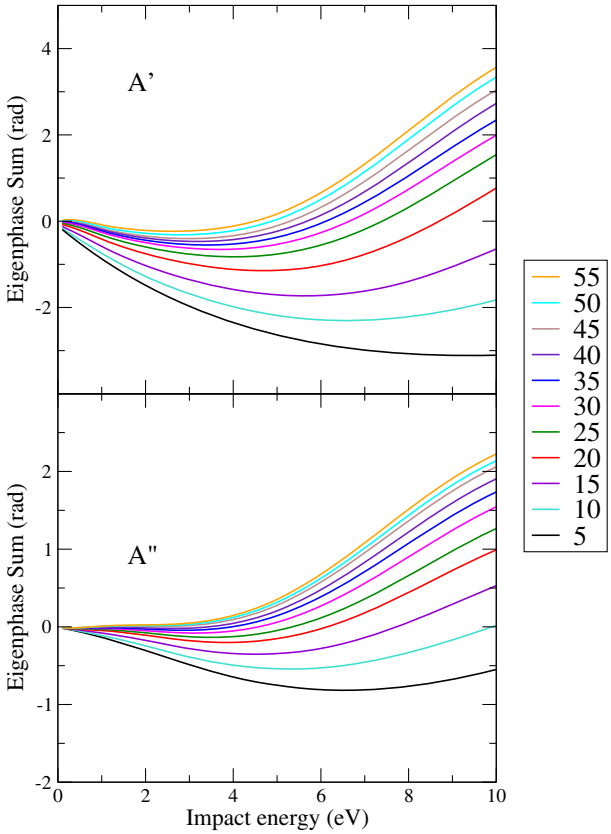

Fig. 1. (Color online) Eigenphase sums, in radians, for A′ (upper) and A″ (lower) symmetry SEP calculations as a function of the number of virtual orbitals retained in the calculation.

SEP calculations which included 35 virtual orbitals give well-converged differential cross sections (DCS). As will be shown below these DCS agree very well with the observation for forward scattering but do not reproduce the apparent rise observed in the DCS in the backward direction. A number of SEP-level studies were undertaken to try and identify the cause of this behaviour. Besides those already discussed above, these considered increasing $\ell_{\max}$ above the standard value of 4 and the inclusion of polarisation effects in the outer region by explicitly adding an $-\alpha_0/R^4$ term to the long-range potential. The experimental value of spherical polarisability $\alpha_0 = 34.5$ a_0^3 [34] was used for this. Including such a term has been shown to improve the representation of polarisation effects in positron-molecule collision calculations [35,36]. The tests focussed on the DCS since, particularly when changing $\ell_{\max}$, it is necessary to balance this with the corresponding change in the Born correction for a meaningful test. Tests showed that our calculated DCS is rather insensitive to (a) increasing the number of virtual orbitals used in the SEP calculation beyond 35; (b) increasing $\ell_{\max}$ beyond 4 and (c) the introduction of long-range polarisation. In particular none of these changes leads to any significant increase in the backwards scattering cross section. This is perhaps to be expected since the dominant effect is due to the long-range ethanol dipole which, for high ℓ, is well-represented by the Born correction.

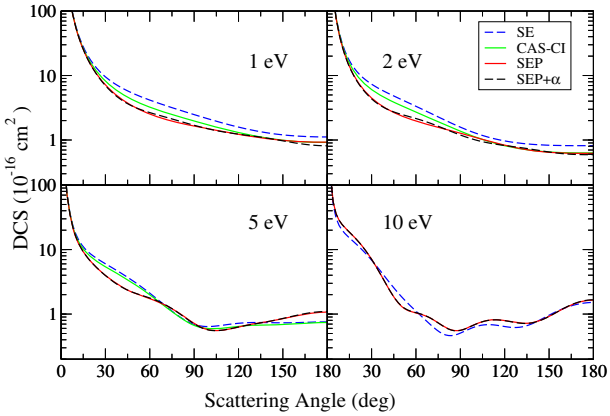

Fig. 2. (Color online) Differential cross sections computed with several models: blue line static exchange (SE); green line CAS-CI close-coupling; red line static exchange plus polarisation (SEP) and black line Static Exchange plus long-range Polarisation (SEP + α).

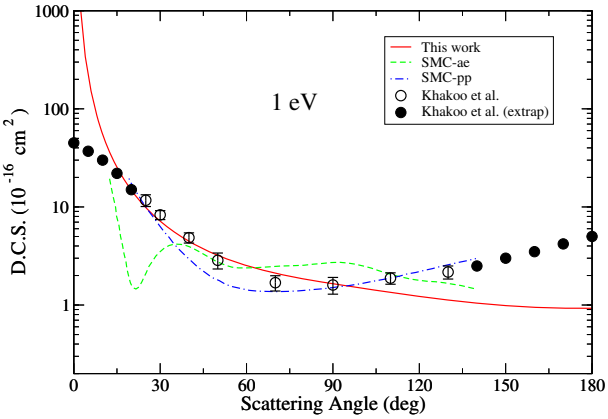

Fig. 3. (Color online) Differential cross section, rotationally unresolved, for collisions of 1 eV electrons with ethanol. Comparisons are made with the measurements of Khakoo et al. [9] and the Schwinger multichannel (SMC) calculations with all electrons (ae) and pseudopotential (pp) reported in the same paper. Note the distinction between experimentally measured points, which have error bars, and extrapolated points at both small and large angles.

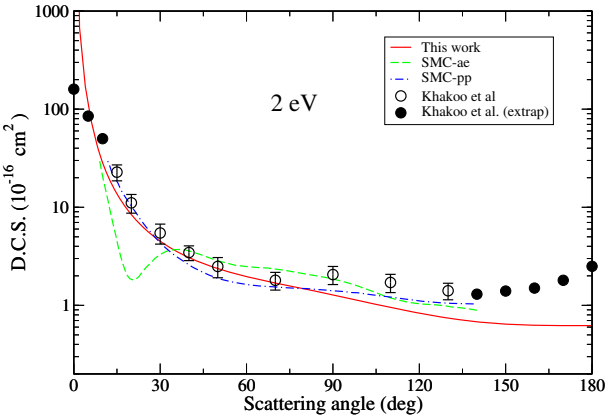

Fig. 4. (Color online) Differential cross section, rotationally unresolved, for collisions of 2 eV electrons with ethanol.

As a further test a variety of CAS-CI target calculations were performed. Again we augmented these calculations with virtual orbitals. However, while all the SE and SEP calculations described above are inexpensive computationally, models with a CAS-CI target and extensive lists of virtual orbitals rapidly become very expensive. The largest calculation we could manage without resorting to very lengthy calculations and special computational procedures [37] involved the use 2 virtual orbitals in the CAS and up to a further 5 virtual orbitals available for L^2 configurations. This, and similar, CAS-CI target models all gave results fairly close to our SE calculations, as illustrated by Figure 2.

As the result of these tests we decided to use an SEP model with $\ell_{\max} = 4$ for 1 to 5 eV and $\ell_{\max} = 5$ for 10 eV. Ethanol's permanent dipole meant that to get a correct description of long-range interaction inclusion of higher partial waves via the Born approximation was vital to represent accurately the DCS at low angles.

3 Results

Figures 3 to 6 present rotationally unresolved, elastic differential cross section calculated in the SEP model and compared with experimental measurements of Khakoo et al. [9], Schwinger multichannel (SMC) calculations from the same paper and the calculations of Lee et al. [16]. To clarify the analysis and discussion of the experimental measurements these are separated in two sub sets: open circles with error bars represent actual measured data while full circles correspond to extrapolated experimental results by Khakoo et al. This extrapolation is necessary to obtain the integrated cross section as it is difficult to make measurements at forward and backward angles. The SMC results were obtained from two different computational implementation: SMC-ae is a parallel computer code in which all electrons are taken into account explicitly and SMC-pp is a version which the core electrons are substituted by a pseudo-potential and only valence electrons are explicitly described. These SMC calculations, which also included a Born correction, show some fairly large differences, especially at the lower energies. The discrepancies between the SMC-ae and the SMC-pp calculations were tentatively attributed to the use of different polarization potentials and partial wave cut-offs in the Born corrections [9].

At low energies our calculated DCS shows excellent agreement the actual experimental measurements (open circles) at angles up to 90°, see Figures 3 and 4. Although SMC-pp calculation reproduces the experimental data at 110° and 130°, our DCS show better quantitative agreement at low angles where the DCS is larger and therefore more important for estimating the integral cross section (ICS).

At 5 eV, see Figure 5, our DCS shows qualitative agreement with the measured experimental data at all angles

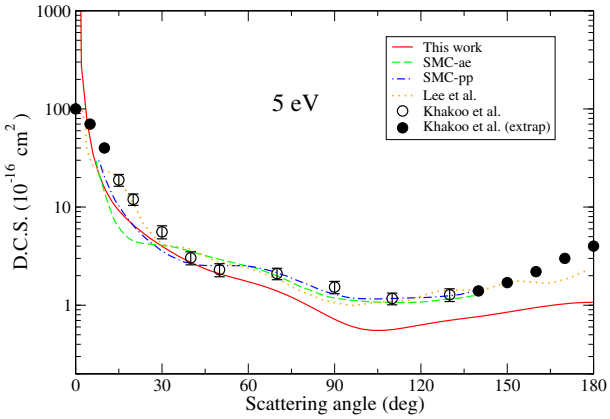

Fig. 5. (Color online) Differential cross section, rotationally unresolved, for collisions of 5 eV electrons with ethanol. Comparisons are made with the measurements of Khakoo et al. [9] and the Schwinger multichannel (SMC) calculations with all electrons (ae) and pseudopotential (pp) reported in the same paper, as well as the calculations of Lee et al. [16].

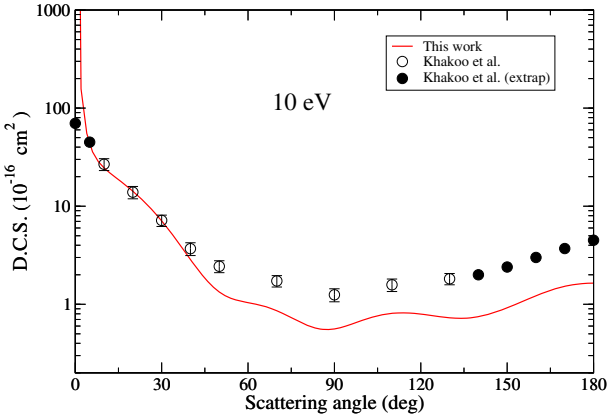

Fig. 6. (Color online) Differential cross section, rotationally unresolved, for collisions of 10 eV electrons with ethanol. Comparisons are made with the measurements of Khakoo et al. [9]; note the distinction between experimentally measured points, which have error bars, and extrapolated points at both small and large angles.

but is lower at both low and high angles. We note that both SMC and Lee et al.'s [16] calculations predict a DCS close to ours at low angles but give good agreement with the measurements at high angles.

Figure 6 shows a comparisons between our $\ell_{\max} = 5$ DCS and the experimental results; there are no published calculations at this energy. We can see that at this higher energy the DCS is increasingly structured and that all structures present in experimental data also appear in our calculated results, for example, there is a good agreement in the minimum position. Again our results are in excellent accord with the actual measurements below 40°. Even though our results are systematically lower at higher angles, we also agree qualitatively with the behaviour of extrapolated experimental results.

Our calculated elastic (rotationally unresolved) ICS is displayed in Figure 7 and compare them with previous

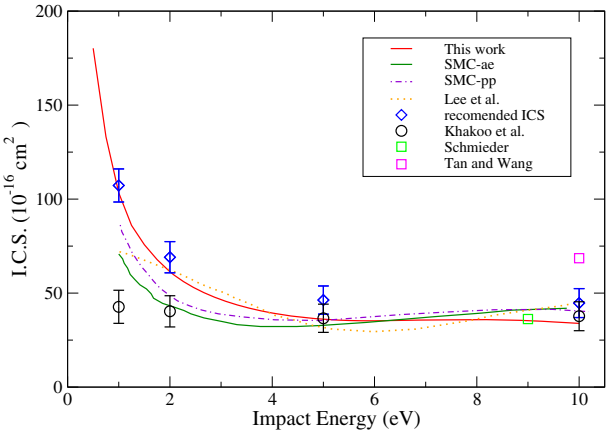

Fig. 7. (Color online) Elastic cross section for electron collisions with ethanol. Comparisons are made with the measurements of Khakoo et al. [9] and Schmieder [3], and the calculation of Tan and Wang [11], Lee et al. [16] and the SMC calculations of Khakoo et al. See text for discussion of the recommended values.

results. Our ICS agrees with the estimated ICS of Khakoo et al. [9] at 5 and 10 eV. This agreement may be partly due to cancellation of errors given that our DCS is lower than the (actual or extrapolated) measurements at large angles but higher then them at low angles. The very old measurement of Schmieder [3] is in remarkable agreement with these results. The ICS calculated using the additivity rule [11] is higher than all other values suggesting that this approximate method is not adequate at low energies.

Rather surprisingly Khakoo et al.'s ICS remains approximately constant at low energies rather than, as would be expected in a strongly dipolar system, increasing rapidly as the collision energy tends to zero. This behaviour can be directly attributed to the form of the low-angle (θ) extrapolation used to augment the set of measured DCS values. The strong low-angle peak in the DCS makes the ICS very sensitive to this region and the extrapolations appear to be significantly too low at very small angles. Even though the DCS is weighted by $\sin(\theta)$ when integrated and therefore tends to zero as θ tends to zero, nevertheless the high value of theoretical DCS at very low angles produces a significant contribution to the ICS. This behaviour has been noted before [12–14] where the solution has been to use Born-corrected calculations to simulate the low-angle behaviour rather than extrapolation of experimental results. It is this approach that we use here.

Our calculations predict much larger ICS at 1 and 2 eV, than those given by Khakoo et al. At these energies the contribution of the low-angle DCS is clearly important for the ICS because of the long-range nature of interaction due to dipole. We therefore expect that the our DCS to give a better representation of the behaviour as θ tends to zero than the assumed experimental extrapolation. We therefore recommend another set of values for ICS that we consider should be much closer to the true value. The new ICS was obtained by integrating the experimental values

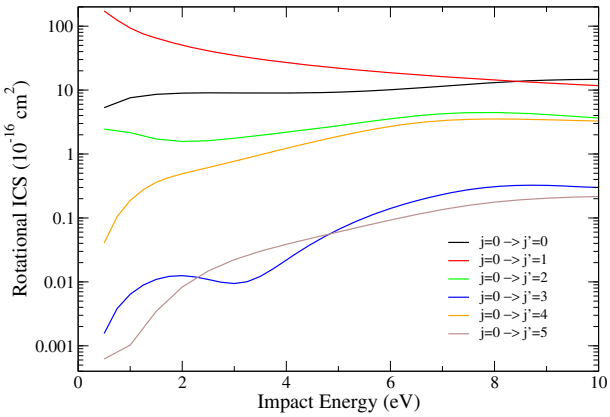

Fig. 8. (Color online) Calculated electron impact rotational excitation cross sections for ethanol.

from $\theta_{\min}$ to 180° and augmenting it with our calculated value integrated over the range 0° to $\theta_{\min}$, where $\theta_{\min}$ is lowest angle for which experimental data is available at the energy under consideration. This procedure neglects the discrepancy between our calculations and both the extrapolated and actual experimental DCS at large angles. However the contribution to the ICS from these large angles is fairly small and in practice using either approach leads to small changes relative to the experimental error bars. Our recommended ICS set is shown in Figure 7 with the same experimental error bars as given by Khakoo et al. The differences between the recommended ICS and our calculated values are fairly small and are due to our DCS being lower at large angles. We note that these large angles are much more important for the momentum transfer cross sections. Estimates of this cross section using the measurements and extrapolations of Khakoo et al. do indeed give answers for this cross section of about twice our calculated values.

Finally, Figure 8 gives our calculated values for the electron impact rotational excitation cross sections. As expected [38], at low energy $j = 0 \rightarrow 1$ excitations predominate. However above 8.5 eV rotationally elastic ($j = 0 \rightarrow 0$) cross sections actually become the largest.

4 Discussion

The results above have concentrated on getting correct low-angle results and hence good values for the integral elastic cross sections. However there are two aspects of the problem which merit further analysis. First is our apparent underestimate of the DCS at large angles and the second is resonance effects in electron ethanol collisions.

We performed a series of calculations at the SE, SEP and close-coupling level but none of these studies gives the increase in the DCS at large angles which is inferred from the experimental results at all energies up to 10 eV. It is unclear from our calculations what mechanism would lead to this increase. However, although the SEP model is good for representing polarisation effects, it is hard to demonstrate that these are actually converged within this model. Furthermore, the constraints of the R-matrix method mean that the virtual orbitals are localised well inside the R-matrix sphere. Our SEP calculations therefore really represent polarisation effects at short-range where they are the strongest. Our tests showed that long-range polarisation effects, defined as those occurring when the electron is outside the R-matrix sphere, are very small. However there is an intermediate region where the effects of polarisation are probably less well modelled in our calculations. It is therefore possible that the systematic inclusion of polarisation effects via, for example, an R-matrix plus pseudostates calculation [39,40], which can recover polarisation at short-, intermediate- and long- ranges [41], would alter the calculated large angle behaviour. However such calculations remain computationally expensive and have yet to be attempted for a target as large as ethanol.

For angles below 90° our calculations are generally in very good agreement with the measured (as opposed to extrapolated) DCSs. The exception is at 5 eV where the agreement is only fair. Our calculations suggest that there are very broad resonance features of both ^{2}A′ and ^{2}A″ symmetry which span the 5 eV region. In the region of a resonance it is to be expected that the DCS will be sensitive not only to the precise representation of the resonance but also, probably, to vibrational effects which we have not considered.

Ibănescu et al.'s analysis of their DEA and VE measurements for ethanol [7] led them suggested that ethanol displays very short-lived σ^* OH shape resonance at 2.88 eV and another short-lived σ^* CH shape resonance around 7.5 eV; these features were augmented by Feshbach resonances at 6.0, 7.7 and 8.8 eV. Our calculations are not designed to characterise Feshbach resonances at energies near the electronic excitation thresholds but should give a reasonable representation of any shape resonance in the system. Our SEP calculations show broad resonances features at about 7.5 eV (^{2}A″ symmetry) and 8 eV (^{2}A′). However the presence of a resonance in both symmetries is not really consistent σ^* resonance and our calculations suggest that these resonance are predominantly f-wave in character. Conversely our study found no evidence for any shape resonances at lower energies. Our results therefore appear to be more in line those of Orzol et al. [8] who observed two broad resonances at about 5.5 and 8 eV. Finally we note that while the previous SMC calculations [9] failed to find evidence for any resonances, Lee et al. [16] comment that they find a broad resonance of each symmetry near 10 eV.

4.1 Conclusions

We present a study of electron collisions with ethanol up to energies of 10 eV. Comparison of our differential cross sections with the measurements of Khakoo et al. [9] give generally good agreement at forward angles, where the cross sections are much the largest, but do not support the extrapolation procedure used at forward angles to allow the measurements to be used to give integrated elastic cross sections. Use of the calculated low-angle differential

cross sections, where experimental measurements are not possible, when combined with the measured cross sections for other angles leads to significantly increased integrated cross sections at low energies. We suggest that these give a much more realistic estimate of the rotationally unresolved, elastic integral electron collision cross sections for ethanol.

Electron impact rotational excitation cross sections are important for applications such as studies of the interstellar medium [42] but are extremely difficult to measure [43]. Our calculations therefore give the first values for this process in ethanol. Finally our study finds two, very broad resonances in qualitative agreement with the dissociative electron attachment results of Orzol et al. [8].

M.M.F. thanks the Brazilian agencies CNPq (Conselho Nacional de Desenvolvimento Científico e Tecnológico) for a scholarship, and Fundação Araucária for partial support.

References

1. J.R. Moreira, J. Goldemberg, Energy Policy **27**, 229 (1999)
2. V. Thomas, A. Kwong, Energy Policy **29**, 1133 (2001)
3. F. Schmieder, Z. Elektrochem. Angew. Phys. Chem. **36**, 700 (1930)
4. R. Feng, C. Brion, Chem. Phys. **282**, 419 (2002)
5. R. Rejoub, C. Morton, B. Lindsay, R. Stebbings, J. Chem. Phys. **118**, 1756 (2003)
6. V.S. Prabhudesai, A.H. Kelkar, D. Nandi, E. Krishnakumar, Phys. Rev. Lett. **95**, 143202 (2005)
7. B.C. Ibănescu, O. May, A. Monney, M. Allan, Phys. Chem. Chem. Phys. **9**, 3163 (2007)
8. M. Orzol, I. Martin, J. Kocisek, I. Dabkowska, J. Langer, E. Illenberger, Phys. Chem. Chem. Phys. **9**, 3424 (2007)
9. M.A. Khakoo, J. Blumer, K. Keane, C. Campbell, H. Silva, M.C.A. Lopes, C. Winstead, V. McKoy, R.F. da Costa, L.G. Ferreira, M.A.P. Lima, M.H.F. Bettega, Phys. Rev. A **77**, 042705 (2008)
10. D.G.M. Silva, T. Tejo, J. Muse, D. Romero, M.A. Khakoo, M.C.A. Lopes, J. Phys. B: At. Mol. Opt. Phys. **43** (2010)
11. Xiao-Ming Tan, De-Hua Wang, Nucl. Instr. Methods Phys. B **269**, 1094 (2011)
12. A. Faure, J.D. Gorfinkiel, J. Tennyson, J. Phys. B: At. Mol. Opt. Phys. **37**, 801 (2004)
13. H. Silva, J. Muse, M.C.A. Lopes, M.A. Khakoo, Phys. Rev. Lett. **101**, 033201 (2008)
14. M.A. Khakoo, H. Silva, J. Muse, M.C.A. Lopes, C. Winstead, V. McKoy, Phys. Rev. A **78**, 052710 (2008)
15. R. Zhang, A. Faure, J. Tennyson, Phys. Scr. **80**, 015301 (2009)
16. M.T. Lee, G.L.C. de Souza, L.E. Machado, L.M. Brescansin, A.S. dos Santos, R.R. Lucchese, R.T. Sugohara, M.G.P. Homem, I.P. Sanches, I. Iga, J. Chem. Phys. **136**, 114311 (2012)
17. D.T. Stibbe, J. Tennyson, Chem. Phys. Lett. **308**, 532 (1999)
18. J. Tennyson, Phys. Rep. **491**, 29 (2010)
19. N.T. Padial, D.W. Norcross, L.A. Collins, J. Phys. B: At. Mol. Opt. Phys. **14**, 2901 (1981)
20. M.A. Morrison, Adv. At. Mol. Phys. **24**, 51156 (1988)
21. F.A. Gianturco, A. Jain, Phys. Rep. **143**, 347 (1986)
22. N. Sanna, F.A. Gianturco, Comput. Phys. Commun. **114**, 142 (1998)
23. J. Tennyson, D.B. Brown, J.J. Munro, I. Rozum, H.N. Varambhia, N. Vinci, J. Phys.: Conf. Ser. **86**, 012001 (2007)
24. J.M. Carr, P.G. Galiatsatos, J.D. Gorfinkiel, A.G. Harvey, M.A. Lysaght, D. Madden, Z. Masin, M. Plummer, J. Tennyson, Eur. Phys. J. D **66**, 58 (2012)
25. S. Coussan, Y. Bouteiller, J.P. Perchard, W.Q. Zheng, J. Phys. Chem. A **102**, 5789 (1998)
26. J.C. Pearson, K.V.L.N. Sastry, M. Winnewisser, E. Herbst, F.C. De Lucia, J. Phys. Chem. Ref. Data **24**, 1 (1995)
27. *CRC Handbook of Chemistry and Physics*, edited by R.C. Weast, 58th edn. (CRC Press, Boca Raton, 1977)
28. J. Tennyson, J. Phys. B: At. Mol. Opt. Phys. **29**, 6185 (1996)
29. A. Faure, J.D. Gorfinkiel, L.A. Morgan, J. Tennyson, Comput. Phys. Commun. **144**, 224 (2002)
30. S. Caprasecca, J.D. Gorfinkiel, D. Bouchiha, L.G. Caron, J. Phys. B: At. Mol. Opt. Phys. **42**, 095205 (2009)
31. Z. Masin, J.D. Gorfinkiel, J. Chem. Phys. **135**, 144308 (2011)
32. J. Tennyson, C.J. Noble, Comput. Phys. Commun. **33**, 421 (1984)
33. D.T. Stibbe, J. Tennyson, J. Phys. B: At. Mol. Opt. Phys. **29**, 4267 (1996)
34. C.G. Gray, K.E. Gubbins, *Theory of Molecular Fluids*, in *Fundamentals* (Clarendon Press, Oxford, 1984), Vol. 1
35. G. Danby, J. Tennyson, J. Phys. B: At. Mol. Opt. Phys. **23**, 1005 (1990),
36. G. Danby, J. Tennyson, J. Phys. B: At. Mol. Opt. Phys. Erratum **23**, 2471 (1990)
37. J. Tennyson, J. Phys. B: At. Mol. Opt. Phys. **37**, 1061 (2004)
38. A. Faure, J. Tennyson, Month. Not. R. Astron. Soc. **325**, 443 (2001)
39. J.D. Gorfinkiel, J. Tennyson, J. Phys. B: At. Mol. Opt. Phys. **37**, L343 (2004)
40. J.D. Gorfinkiel, J. Tennyson, J. Phys. B: At. Mol. Opt. Phys. **38**, 1607 (2005)
41. M. Jones, J. Tennyson, J. Phys. B: At. Mol. Opt. Phys. **43**, 045101 (2010)
42. I. Jimenez-Serra, J. Martin-Pintado, S. Viti, S. Martin, A. Rodriguez-Franco, A. Faure, J. Tennyson, Astrophys. J. **650**, L135 (2006)
43. D. Shafir, S. Novotny, H. Buhr, S. Altevogt, A. Faure, M. Grieser, A.G. Harvey, O. Heber, J. Hoffmann, H. Kreckel, L. Lammich, I. Nevo, H. Pedersen, H. Rubinstein, I.F. Schneider, D. Schwalm, J. Tennyson, A. Wolf, D. Zajfman, Phys. Rev. Lett. **102**, 223202 (2009)